

**BIOMEDICAL**  
ENGINEERING

---

**Carnegie Mellon University**

**2015 Biomedical Engineering  
Summer Undergraduate Research Symposium**

**July 28, 2015**

**Wean Hall 5415**

**9:00 AM to 1:30 PM**

## **Biomedical Engineering at Carnegie Mellon University**

Biomedical engineering education at Carnegie Mellon reflects the belief that a top biomedical engineer must be deeply trained in both a traditional engineering practice and biomedical sciences. The unique additional major program leverages extensive collaborations with sister departments in the College of Engineering and with major medical institutions in Pittsburgh. This collaborative approach, combined with a rigorous engineering education, confers unique depth and breadth to the education of Biomedical Engineering graduates.

## **Biomedical Engineering Summer Undergraduate Research Program (BME-SURP)**

This program allows students to spend a ten-week period on a project that combines translational research and clinical exposure at a local medical center. Hundreds of students have participated in BME-SURP since its introduction in 1980. The experience have played a major role in helping students choose their career paths and obtain positions in industrial or academia. This program is supported by grants from the CMU College of Engineering, Merck & Co., Inc., and the CMU University Research Office (URO).

## **Carnegie Heart Program**

The Carnegie Heart Program is a collaborative effort between the Biomedical Engineering Department at Carnegie Mellon University and the Allegheny Health Network. The purpose of this program is to develop biomedical engineers who can apply their education toward new technologies for clinical cardiovascular medicine. In addition to students' experience in a laboratory setting, students will shadow cardiovascular clinicians at Allegheny General Hospital one day every two weeks. This program is supported through a grant from the American Heart Association.



## **Presentation Schedule**

### **8:30 AM to 9:00 AM            Continental Breakfast**

9:00 AM to 9:15 AM            Alexandra Cerny

9:15 AM to 9:30 AM            James Ham

9:30 AM to 9:45 AM            Gordon Pace

9:45 AM to 10:00 AM          Gillian Crews

10:00 AM to 10:15 AM          Prarthana Joshi

10:15 AM to 10:30 AM          Maryam Aghadi

### **10:30 AM to 10:45 AM          Break**

10:45 AM to 11:00 AM          Marissa Morales

11:00 AM to 11:15 AM          Veronica Jaime-Lara

11:15 AM to 11:30 AM          Patricia Pan

11:30 AM to 11:45 AM          Derek Loh

11:45 AM to 12:00 PM          Sabrina Liu

12:00 PM to 12:15 PM          Rachel Freer

12:15 PM to 12:30 PM          Hsuan (Michelle) Ma

12:30 PM to 12:45 PM          Nicole Bustos

### **12:45 PM to 1:30 PM          Lunch and cake!**

Note: Muyuan Li and Megan Pedulo presented earlier in a separate presentation

**Alexandra Cerny**

Advisor: Kris Dahl, Ph.D.

BME-SURP

Muscular dystrophies are a class of genetic disorders that affect children and adults through the weakening and destruction of muscle tissue, including skeletal and cardiac muscle. A subclass of muscular dystrophies, called Emery Dreifuss muscular dystrophy (EDMD), are caused by malfunctions within the nuclear force transduction network that cause structural defects within the cell. We have shown a preliminary link between the structural proteins emerin, lamin A and spectrin and the ability of the cell to deform and reform from strain. However, there has not been a rigorous quantification and correlation of protein level and mechanical response of cells. For a proper mechanical model, we need to consider the full structure of the protein networks and how this network influences mechanics. Here we investigate the individual effects of proteins within the force propagation network through multiple different mechanical assays. The stretching assay tests the cell's ability to maintain its shape under strain caused by stretching the cells on a substrate. The effects of tensile strain on the movement and shape of the cell can also be measured using a micropillar assay. It has been found that cells lacking the main connection between the nucleus and the cytoskeleton are unable to move smoothly through the micropillars and often get stuck with the nucleus lagging at the back end of the cell. Cell area and circularity will be analyzed in the future in order to observe any changes that may occur in these factors as a result of the various protein knockdowns. In performing this research, we hope to characterize the different effects of each protein within the force propagation network such that targeted treatment can be given to those who experience the effects of their malfunctioning.

## James Ham

Advisor: Olivia Finn, Ph.D. (University of Pittsburgh School of Medicine, Department of Immunology)  
BME-SURP

### 4-1BB co-stimulatory domain reduces tonic signaling for biotin-binding immune receptors (BBIR)

#### Introduction:

Chimeric antigen receptors (CAR) are artificial T cell receptors that use the specific binding capabilities of antibodies to direct engineered T cells to lyse target cells that display a tumor-associated antigen (TAA). Developing CARs targeting a repertoire of TAAs is an active area of research, but each CAR is only capable of recognizing one TAA. To develop an immunotherapeutic capable of a flexible response to multiple expressed TAAs, a variant of the CAR whose binding domain has been replaced by avidin was constructed. These variants are called biotin-binding immune receptors (BBIR), and have been shown to become activated in the presence of biotinylated antibodies bound to their target antigen, and demonstrate specific target cell lysis<sup>1</sup>. It was found that certain BBIR constructs would lead to tonic signaling which would constitutively activate T cells, leading to the up-regulation of T-cell exhaustion markers and causing a poor response to TAAs. It was this project's objective to develop a BBIR based on published work that would exhibit greater specificity and target cell killing than previously done.

#### Materials and Methods:

Multiple BBIR expression plasmids were constructed using traditional restricting enzyme/ligation cloning and isothermal Gibson assembly cloning techniques. The binding domain consisted of an engineered monomeric streptavidin (mSA) which had demonstrated a 200-fold increase in binding affinity compared to dimeric chicken streptavidin<sup>2</sup>. Monoclonal antibodies derived from patients immunized with a MUC1 vaccine were biotinylated and utilized in all assays. BBIRs with various co-stimulatory domains were constructed. Jurkat cells were transduced to express BBIRs then stained with anti-MUC1 mAb for 30 minutes then co-incubated with Jurkat cells expressing aberrant MUC1 for 24 hours in DMEM. The cells were then assayed for activation markers CD69 and CD62L.

#### Results and Discussion:

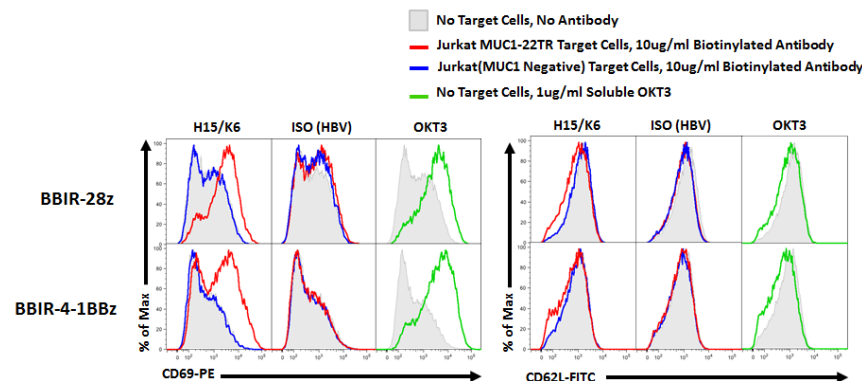


**Figure 1.** Activation assays for CD69 and CD62L for BBIRs with either CD28 and 4-1BB co-stimulatory domains after being co-incubated with target cells for 24 hours. BBIR-4-1BB transduced cells displayed a lower level of tonic signaling compared to their CD28 counterparts.

It was found that BBIR constructs with CD28 co-stimulation would indiscriminately activate T cells regardless of whether they were in the presence of aberrant MUC1 or not. 4-1BB co-stimulation did not activate these cells. Supernatant taken from these cultures and assayed for IL-2 showed that there was less produced in 4-1BB cultures compared to CD28 cultures.

#### Conclusions:

Based on the above results, 4-1BB costimulation leads to a lower amount of tonic signaling. This has implications in future experiments, making this BBIR construct the preferred one for testing in primary cells. It is hoped that CARs and BBIRs will continue to exhibit a strong level of similarity in the signaling domain construct.

#### Acknowledgements:

Special thanks to Jason Lohmueller, PhD for his assistance.

#### References:

1. Lipowska-Bhalla, Grazyna, David E. Gilham, Robert E. Hawkins, and Dominic G. Rothwell. "Targeted Immunotherapy of Cancer with CAR T Cells: Achievements and Challenges." *Cancer Immunology, Immunotherapy* 61.7 (2012): 953-62.
2. Lim, Kok Hong, Heng Huang, Arnd Pralle, and Sheldon Park. "Stable, High-affinity Streptavidin Monomer for Protein Labeling and Monovalent Biotin Detection." *Biotechnology and Bioengineering* 110.1 (2013): 57-67.

## Gordon Pace

Advisor: Tzahi Cohen-Karni, Ph.D.  
BME-SURP

### E-nanomesh for Sensing and Culturing Electroactive Cells

**Introduction:** Nanostructures and nanostructured substrates show enhanced coupling to artificial membranes, cells, and tissue. Such nano-bio interfaces exist at a length scale natural for biological systems and offer better sensitivity and spatial resolution as compared to conventional planar structures. In this work, we report the synthesis and electrical properties of silicon nanowires (SiNWs) based electronic mesh (e-mesh) platform. The SiNW e-mesh could prove useful for fundamental studies of cells-surface interactions, measuring the electrical activity of cells in 3-demiensions, real-time drug assays, and creation of semiconductor/muscle hybrids for controlling prosthetic limbs.

**Materials and Methods:** SiNWs were synthesized using vapor-liquid-solid growth method (VLS). Gold nanoparticles (AuNPs) catalysts were immobilized on a silicon substrate using poly-L-lysine. Synthesized nanowires were collapsed into a mesh by pouring liquid nitrogen over their surface, while the samples were still in the quartz tube of the synthesis system. After collapsing the wires, an additional CVD process of either shell growth or thermal annealing was performed to fuse the wires together into a continuous, highly conducting e-mesh. A scanning electron microscope (SEM) was used to check the success of NW synthesis, confirm that the liquid nitrogen did indeed collapse the wires into a mesh, and evaluate the continuity the mesh. Four point probe measurements were used to characterize the electrical properties of the mesh (by using Keithley 2401 source meter measurement set up).

**Results and Discussion:** SEM images indicated growth conditions of 150 minutes at 420°C or 100 minutes at 450°C yield NWs longer than 50  $\mu\text{m}$ . NWs of this length, or longer, are desired because they collapse into a thick mesh that can readily grow cells and be lifted off the growth substrate. Application of liquid nitrogen was a successful method for collapsing wires into a mesh. Samples synthesized using these conditions typically had meshes 8  $\mu\text{m}$  thick. The CVD shell process created a continuous mesh by forming an additional silicon layer around the NW cores. The presence of this shell is evidenced by the thicker wires in Figure 1(b) compared to Figure 1(d). The CVD shell process was also observed to deposit a layer of silicon on the surface of the growth substrate, as seen in Figure 1(a). This layer interferes with electrical measurements of the mesh because some of the resistance measured will be due to the silicon layer rather than the mesh itself. This prompted a sample to be synthesized without a shell. The NWs of this sample were fused via thermal annealing at 700°C. As seen in Figure 1(c), this resulted in less silicon deposition on the substrate surface. SEM images of a control, non-thermally annealed sample revealed that sections were not completely collapsed, the wires did not appear to be fused, and the wires moved when exposed to the electron beam of the SEM, all of which indicate the NWs were not connected to form a continuous mesh. Preliminary four point probe measurements show that the n-doped thermally annealed sample has a sheet resistance two orders of magnitude smaller than both the non-thermally annealed sample and the intrinsic sample ( $4 \times 10^{-3} \Omega/\text{sq}$  vs  $9 \times 10^{-5} \Omega/\text{sq}$  and  $6 \times 10^{-5} \Omega/\text{sq}$ , respectively).

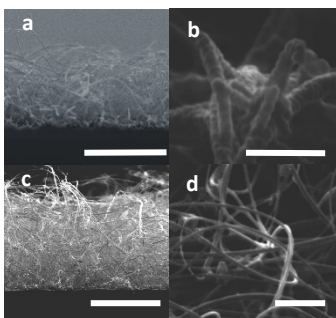


**Figure 1.** SEM images of e-meshes. **a)** 90° view of heavily doped n-type SiNWs, grown at 420° C for 150 minutes, collapsed with liquid nitrogen, followed by CVD shell deposition process at 775° C for 20 minutes. 20 nm AuNPs catalyst. 4 mm scale bar **b)** Expanded view of (a). 400 nm scale bar **c)** 90° view of heavily doped n-type SiNWs, grown at 450° C for 100 minutes, collapsed with liquid nitrogen, thermally annealed at 700° C for 10 minutes. 20 nm AuNPs catalyst. 5mm scale bar **d)** Expanded view of (c). 500 nm scale bar

**Conclusions:** Liquid nitrogen successfully collapsed free standing SiNWs into a mesh. Thermal annealing fused NWs without forming a layer of silicon on the substrate surface, which occurs to a greater extent during shell growth. Comparison of a thermally annealed sample and a non-thermally annealed sample indicated thermal annealing is both necessary and successful for fusing the nanowires into a continuous mesh. The next steps of this

project will be to successfully characterize the electrical properties of the e-nanomesh and use it as a substrate for culturing cells and chemical sensing applications.

**Acknowledgements:** The author would like to thank Dr. Tzahi Cohen-Karni and Elnatan Mataev for their assistance and guidance with this project.

## Gillian Crews

Advisor: Todd Pryzbycien, Ph.D.

BME-SURP

### The Investigation of PEGylating Protein A Media in Effort to Decrease Non-specific Binding in the Filtration of Monoclonal Antibodies

**Introduction:** In downstream processing for pharmaceuticals, protein A affinity chromatography is crucial step in the filtration of monoclonal antibodies (mAbs). The addition of polyethylene glycol (PEG) chains to the protein A media increases the selectivity of this step by decreasing non-specific binding, however it also decreases the binding capacity of the media. This project inspects to what extent this depression in binding capacity occurs, and how to optimize mAbs processing through PEGylating. Experimental conditions are made to directly correlate to those that would be seen in industrial protein A packed beds.

**Materials and Methods:** There are two methods used to inspect how PEGylating affects the binding capacity of protein A media. These two setups allow inspection of how mAbs binding takes place in static and dynamic conditions. With the static case, protein A media is added to Immunoglobulin G (IgG) solution and they are allowed to mix for 24 hours, allowing for the determination of the maximum binding capacity of the media. In the dynamic case, kinetics of the process can be determined by watching the adsorption take place in real time. This is completed by taking the UV absorbance reading of IgG solution that is being mixed with protein A continuously over the course of two hours.

Each method was performed on both modified and unmodified media to allow for comparison between traditional and PEGylated protein A. The PEGylated media was further inspected by looking into the effects of PEG chain length and extent of PEGylation on binding capacity.

**Results and Discussion:** To determine the binding capacity, a plot of adsorbance of IgG on protein A media vs. concentration of the IgG solution was formed and fit to a Langmuir isotherm. The asymptote of the isotherm models the maximum binding capacity of protein A media. It was found that unmodified media does have the highest binding capacity, with 99.8 mg IgG adsorbed per mL protein A media. High extent PEGylated media, with about three 5 kDa PEG chains attached to each protein A particle had a significantly lower binding capacity of 66.7 mg/mL. With the low extent case, there was on average one 5 kDa PEG chain attached to each protein A particle, and the binding capacity was found to be 81.1 mg/mL. Additionally, low extent media with only 65% of protein A molecules having a single 20 kDa PEG chain attached had a lowered binding capacity of 66 mg/mL.

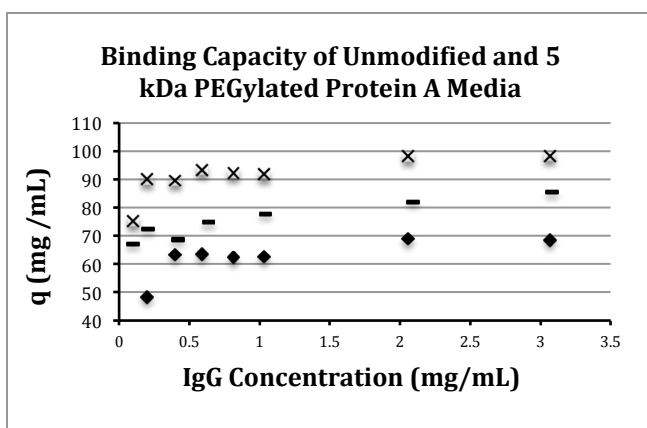


**Figure 1:** The binding capacity of low extent 5 kDa PEGylated protein A media (-) is 20% lower than that of unmodified media (×) and high extent 5 kDa PEGylated media (w) has a binding capacity 35% lower than that of unmodified media.

**Conclusions:** PEGylation of protein A media to decrease non-specific binding in mAbs filtration will also result in a notable decrease in the media's binding capacity for mAbs. This decrease in binding capacity becomes more severe as the extent to which the media is PEGylated increases and as the length of PEG chains increases.

**Acknowledgements:** Special thanks to Justin Weinberg for his assistance.

## Prarthana Joshi

Advisor: Keith Cook, Ph.D.

PES Institute of Technology

### *Pseudomonas aeruginosa* biofilm growth analysis

**Introduction:** Cystic fibrosis (CF) is a chronic, autosomal disorder resulting in thick, viscid mucus that adheres to the airways. This causes decreased mucociliary clearance and impaired host defense. Bacteria, like *Pseudomonas aeruginosa*, form a biofilm on the dehydrated mucus in the lungs leading to bronchiectasis. The aim of our research is to expose the biofilm to antibiotics emulsified in perfluorocarbon (PFC). In the lab, we are recreating the biofilms on a cellulose membrane in a bioreactor. My work involved determining the best ways to quantify the biofilm growth and to establish how often the media needs to be changed in the bioreactor.

**Materials and Methods:** A bacterial colony was obtained from streaked plates of LB-agar and inoculated into a 50ml conical containing 20ml of tryptic soy broth with 1% glucose. This was incubated in a shaker for 7 h 30 min at constant speed at 37 °C. Samples were collected every 30 minutes and the optical density (OD) was measured for each sample at 600nm using a spectrophotometer. A graph of OD vs time was plotted. When the OD crossed 0.1, 3 ml of the sample was pulled out and transferred to a fresh 15ml conical. The cellulose membrane was cut in two equal halves and placed on an LB-agar plate. The bacterial solution was diluted such that the OD was 0.1 and 250µl was spread onto each half of the membrane. The biofilm was allowed to grow for 24 hours in an incubator. The membranes were then vortexed (for 3 minutes) or scraped and transferred to 10ml media to obtain the biofilm for quantification. The bacterium in media was grown for 6 hours and the OD was measured. Graphs were plotted and Student's t-test was performed to determine significance.

**Results and Discussion:** The bacteria attains log phase (OD ≈ 0.1) at t=180 min. The growth rate of bacteria starts to decrease at t=420 min (Fig.1). This implies the media in the reactor needs to be changed after approximately 7 hours of growth. Regarding the biofilm on the membrane, there was a significant increase in the OD 6 hours after incubation signifying the bacteria is viable after applying both methods (Fig.2). Student's t-test was performed and it showed no significant difference (p=0.64) between the growth of bacteria after scrape and vortex methods. There was lesser bacterium left on the membrane after vortex as compared to scraping (Fig.3).

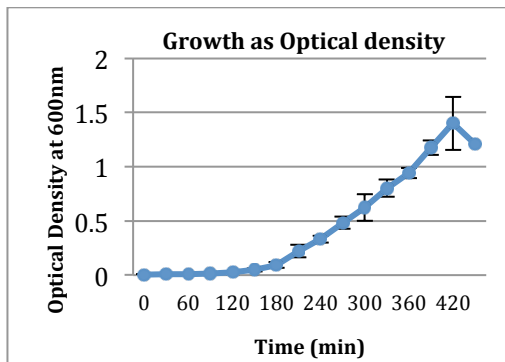


**Fig.1:** Growth of bacteria as Optical Density at 600nm vs time (min)

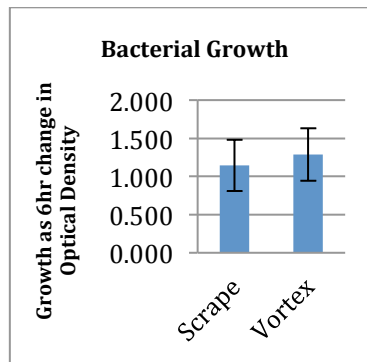


**Fig.2:** Growth of bacteria from membrane after 6 hours of incubation

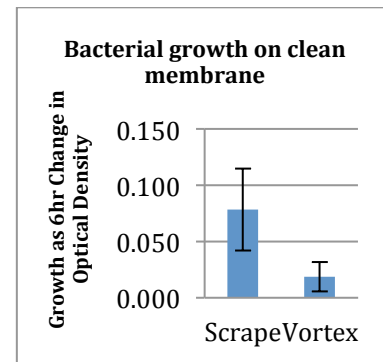


**Fig.3:** Growth on clean membrane after scraping and vortex

**Conclusion:** By analyzing the experimental data, we can conclude that the media in the bioreactor should be changed every 7 hours to ensure bacteria is in log phase and viable. The vortex method is preferred as there is less residual bacterium left on the membrane and it gives us more consistent results.

**Acknowledgements:** This project would not be possible without the guidance of Dr. Keith Cook and Diane Nelson. I would like to thank them for giving me this opportunity to learn and also for their constant encouragement through the course of this internship.

## **Maryam Aghadi**

Advisor: Kris Dahl, Ph.D.

### **Role of the LINC complex in propagating tension within the cell**

Engineering cells and tissues would significantly reduce the health consequences caused due to tissue and organ failure. A functional tissue is a set of many similar and non-similar cells that interact with one other and with the extracellular matrix to perform functions. Particularly in structural tissues, it is important to understand the mechanism of force generation and propagation within the cell as it allows them to accomplish many inter- and intra-cellular tasks. So here we have investigated the role of nucleoskeleton-to-cytoskeleton (LINC) complex in propagating tension within the NIH 3T3 fibroblast cells. In order to test that, we worked on proving the following hypothesis: cells with disturbed LINC complex transmit less force within the cell, which leads to less displacement of the particles within the nucleus over time as compared to the cells with intact LINC complex. In order to test that, LINC complex of the cell was disturbed by expressing a dominant negative KASH domain of the nesprin proteins (DN-KASH), responsible for connecting inner nuclear complex with the cytoskeleton. These (DN-KASH) were expressed by transfected plasmids, purified from DH5- $\alpha$  using Midi prep and transfected into fibroblasts using lipofectamine. Fibroblasts were plated on glass coverslip and the displacement of particles within the nucleus was quantified by carrying out real time fluorescence microscopy. Our results would allow us to expand our research by plating those cells on substrates of varying stiffness and rigidities which would allow us to understand the role of LINC complex in force generation within the organs of various tensile strengths.

## **Marissa Morales**

Advisor: Michael Lotze, Ph.D.

BME-SURP

### **Effect of High Mobility Group Box 1 (HMGB1) in platelets on tumor metastasis**

#### **Introduction:**

Metastasis, or metastatic disease, is the spread of a cancer from one organ to another not directly connected with it. During metastasis some cancer cells acquire the ability to penetrate the walls of the lymphatic or blood vessels. Tumor metastasis is prevented by tumor cells being destroyed in the blood stream either by recognition by the immune system or shear stress. Promotion of metastasis is facilitated by platelets forming complexes with tumor cells.

Platelets are components of the blood that are normally responsible for clotting through means of adhesion and aggregation. Platelets form complexes with tumor cells in the blood to help evade detection from the immune system and to withstand the shear stress of blood flow. Activation of platelets by tumor cells occurs either through direct contact or secretion of platelet activators by tumor cells. However, the relative importance of each activator is still unknown. A reduced level of circulating platelets is beneficial in reducing the degree of tumor metastasis but has adverse effects in blood functionality. In response, a way to hinder the interaction between tumor cells and platelets is desired.

High mobility group box 1, HMGB1, is a non-histone chromosomal protein that plays a number of different roles in inflammation, injury and cancer. HMGB1 has dual roles as an oncogenic factor and tumor suppressor. Activated platelets are a source of HMGB1 which helps to promote autophagy leading to an increased degree of metastasis. A proposed way to decrease tumor metastasis is to evaluate tumor growth in the presence of platelets that do not express HMGB1.

#### **Materials and Method:**

Genetically modified mice were bred with HMGB1 knocked out specifically in platelets. The genotype of the mice was analyzed by isolating the DNA from tail tissue using a DNA isolation kit from QIAGEN. Once isolated, the DNA was amplified using PCR in order to analyze the DNA using gel electrophoresis. Platelets were isolated from the mice by collecting blood from the heart of both wild type and HMGB1 knockout mice. Western blot was used to analyze the presence of HMGB1 in both type of mice.

#### **Results and Discussion:**

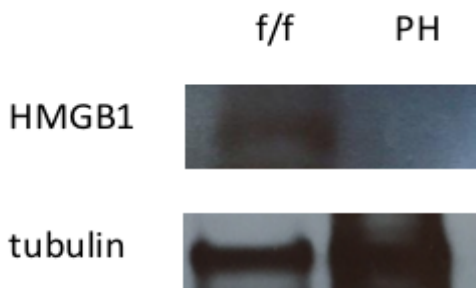


**Figure 1:** Western blot analysis was used on platelet isolated from wild type (f/f) and HMGB1 knockout (PH) mice proving the presence of HMGB1 in the wild type and absence in the knockout mice. Tubulin was used as an internal control.

#### **Conclusion:**

The combination of data collected from the DNA isolation showed that genetically modified mice were successfully breed to have a specific knockout of HMGB1 in the platelets. Platelet isolation and western blot successfully showed the presence of HMGB1 in the wild type mice and

absence in the knockout mice. Further analysis includes injecting mice with tumors to compare the growth in the wild type and knockout mice.

#### **Acknowledgments:**

This author would like to thank Dr. Lotze and his lab staff at the Hillman Cancer Center for their support and help on this project.

## Veronica Jaime-Lara

Advisor: Cameron Riviere, Ph.D.

BME-SURP

### Needle Steering: Optimizing Control Gains

**Introduction:** In current brain surgeries and biopsies, needles are inserted into the brain in straight trajectories. However, steering a needle in curved trajectories improves the quality of the procedure by avoiding crucial areas of the brain. To make this possible, the desired trajectory must be selected before the procedure, and monitored throughout insertion. Due to inherent noise and error, the needle may not always follow the path precisely. To ensure the needle stays as close as possible to the pre-selected path, proportional-integral control can be used. Using computer programming, it is possible to simulate the system and needle movement to find the resulting cross-track error (distance from the path) and heading error (angular orientation relative to the path axis). The main goal of this research project is to minimize these errors by finding optimal proportional and integral control gains.

**Methods:** To optimize gains, a Matlab code was designed to take gain values as input, and output a summary of performance. A summary of the results was created by taking the mean and standard deviation of results in multiple trials. The results were compared based on greatest reduction of overshoot, rise time, settling time, and target accuracy. Selected gain ranges were initially broad and were then narrowed down. First, proportional cross-track gains between 0.001 and 1 versus heading gains between the ranges of 0.0001 and 1 were explored. These were narrowed down in range until a consistently effective value could be selected. Next, cross-track integral gains between 0.0001 and 0.1 were observed. Cross-track proportional gain alone was compared to cross-track integral gain to determine whether integral gain improved results. These various range comparisons are pivotal in finding an optimal gain combination.

**Results and Discussion:** Proportional control was used initially for the experiment and proved effective. The addition of an integral control variable was studied and proved to reduce rise time, but compromised overshoot and settling time. The ideal proportional heading gain was narrowed down between approximately 0.08 and 0.2, the ideal proportional cross-track gain was narrowed down between 0.05 and 0.1, and the optimal integral gain value was determined to be between 0 and 0.01. Due to noise inherent to the system, there is some degree of variation in the output results.

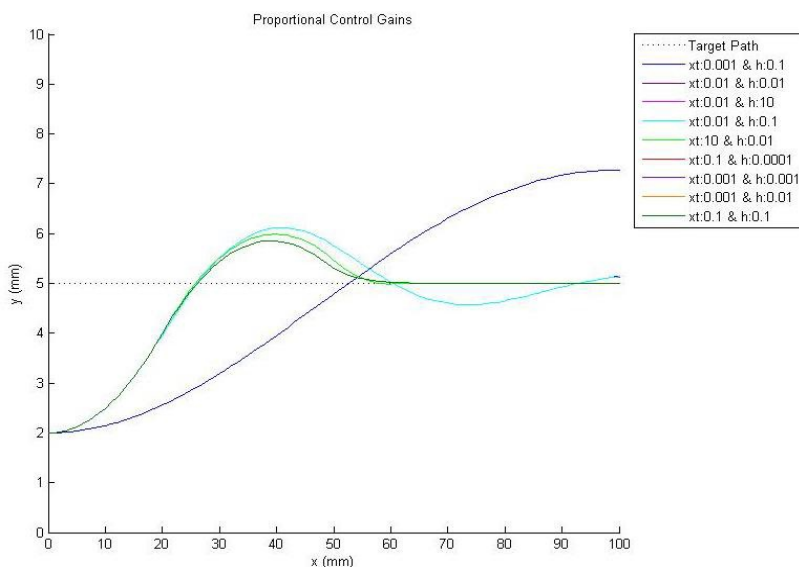


**Figure 1.** The plot to the left depicts the trajectories controlled by various cross-track and heading proportional gains. Some combinations overlap, while others depict different rise times, settling times, and percent overshoot. One path (navy blue) never reaches the target area. In this simulation the target path is straight and has no noise; however, the path is more often curved in shape and contains error.

**Conclusion:** The ideal gain combination includes a cross-track proportional gain of 0.05-0.1, a heading proportional gain of 0.08-0.2, and a cross-track integral gain 0-0.01. These combinations best reduce overshoot, rise time, settling time and target accuracy for needle path following. Therefore this is the most effective control gain combination for keeping the needle as close as possible to a pre-selected path through the brain.

Future research is needed to compare the performance of this gain combination in a realistic environment with that of our simulation.

**Acknowledgements:** Special thanks to Craig Lehoccky for his extensive instruction and guidance, and to Dr. Cameron Riviere & Dr. Conrad Zapanta for providing me the opportunity to work on this project.

## **Patricia Pan**

Advisor: Francois Yu, Ph.D.

BME-SURP

### **Comparing DSPC and DOPE liposome compositions for use in local drug delivery using microbubbles and ultrasound**

Microbubbles (MBs) are microscopic bubbles with a lipid or polymer shell, and are used in conjunction with ultrasound (US) for local drug-delivery. Drugs that have been encapsulated by liposomes are either conjugated to or co-injected with these MBs, and when they reach the target site, an US is passed through the MBs, causing them to oscillate which in turn causes the liposomes to release their payload. DSPC liposomes are the current standard, and this study compares the efficacy of DOPE liposomes to DSPC liposomes in terms of US drug release when conjugated to VO1 2um MBs. DOPE liposomes are known to be more sonosensitive, or more sensitive to the oscillations of MBs, which would correlate to a higher payload release though at the expense of increased instability.

Calcein dequenching assays were used to determine the relative efficacy of DSPC vs. DOPE liposomes. Both types of liposomes were hydrated with a 59429 nm calcein solution, where calcein is a fluorophore that exhibits self-quenching and dequenching. As a result, at high concentrations such as encapsulated in a liposome, calcein is quenched and does not fluoresce, but at lower concentrations, such as when fully released from liposomes due to the addition of a detergent (2.5% Triton-x-100), it emits fluorescent waves that can be read by a fluorometer (Beckman Coulter multimode detector). Drug encapsulation (liposomes) and drug release (liposome conjugated MBs) efficacy were determined via fluorescence readings from dequenching assays. The the stability of DSPC vs. DOPE liposomes, and when conjugated with MBs, were assessed via dequenching assays over time.

In terms of total calcein encapsulation efficiency, DSPC was more efficient at DOPE since its dequenched fluorescence was twice as high as those of DOPE liposomes within the linear range of the calcein fluorescence curve. This higher calcein encapsulation by DSPC can be explained by its larger volume, as it has an average diameter of 228 nm compared to DOPE's 178 nm, resulting in a two-fold increase in volume.

In terms of ultrasound release efficiency, however, DOPE was more effective percent-wise because it released 40% of its load after 90 seconds of 170 ultrasound, compared to DSPC's 30%. Although overall, in terms of total release, DSPC was still more efficacious due to its 4x higher release fluorescence at various US exposures. This makes sense because DOPE is more unstable than DSPC is but encapsulated less calcein.

Overall, DSPC liposome conjugated MBs remain the standard, as they release the most payload between DSPC and DOPE MBs.

Acknowledgements: Special thanks to Flordeliza Villanueva (lab supervisor)

## **Derek Loh**

Advisor: Christopher Bettinger, Ph.D.  
Carnegie Heart

### **Genipin crosslinked fibrin networks to improve endovascular coiling for aneurysm treatment**

#### **Introduction**

An intracranial aneurysm is a localized dilation of a blood vessel in the brain. The risk of rupture of these aneurysms pose a serious health threat for those affected. The current method of treatment, known as endovascular coiling, involves inserting platinum coils through a catheter into the aneurysm to promote clotting. This cuts off blood flow to the damaged part of the vessel and removes the risk of rupture. However, over time, proteolytic activity causes the clot to break down and reintroduce blood flow within the aneurysm. In order to improve endovascular coiling, we plan to use genipin, a naturally derived molecule, to crosslink the fibrin network within the blood clot. The genipin will be delivered to the aneurysm by a thin coating of PLGA on the surface of the platinum coil. The crosslinked fibrin network will resist enzymatic degradation and provide a more permanent treatment for intracranial aneurysms. To test the efficacy of this potential solution, we investigated the effects of genipin on fibrin networks as well as the ability for genipin to release from a thin film of PLGA.

#### **Materials and Methods**

Fibrin hydrogels made from solutions of fibrinogen and thrombin were exposed to solutions of genipin. A rheometer was used to measure the storage moduli of these samples as well as a control (pure fibrin hydrogel). An increase in the storage modulus of the hydrogel is an indicator of successful crosslinking. In order to model the thin PLGA coating that will be on the platinum coil, thin films of genipin and PLGA solution were spin coated onto glass coverslips. A profilometer was used in order to ensure that the PLGA and genipin film was comparable to the 3 micron thick coating on a platinum coil. The coated coverslips were then incubated in PBS to allow for the genipin to diffuse into solution. UV-vis spectroscopy was then used to measure the amount of genipin that released from the films. By taking UV-vis spectroscopy samples over a period of over 72 hours, it is possible to determine both the amount and rate at which genipin releases.

#### **Results and Discussion**

The rheology data showed that exposure to genipin significantly increases the storage moduli of the fibrin hydrogels. The average storage modulus for the control samples was 224 Pa, while the moduli for the samples exposed to 10% and 20% genipin solutions were 1195 Pa and 1068 Pa, respectively. This shows a significant increase in the storage moduli of the hydrogels that were exposed to genipin, suggesting that the samples successfully crosslinked. It is also worth noting that the 10% genipin samples had a higher average storage modulus than the 20% genipin samples. This is likely due to the existence of an optimal concentration for genipin to induce crosslinking.

UV-vis spectroscopy experiments showed that genipin successfully released from the spin coated coverslips. In both the 10% genipin and 20% genipin samples, over 80% of the genipin released from the PLGA in 24 hours. In addition, the linear region of the release curves are similar for all of the samples and suggest that it will be possible to tune a consistent release of the drug from the PLGA. It is predicted that the diffusion coefficient for these samples will be  $6.93 \times 10^{-12} \text{ cm}^2 \text{ s}^{-1}$  for the 10% genipin samples and  $7.20 \times 10^{-12} \text{ cm}^2 \text{ s}^{-1}$  for the 20% genipin samples.

#### **Conclusions**

Genipin was able to crosslink fibrin hydrogels as well as predictably release from a thin film of PLGA. Both of these features make genipin a very promising drug to be used in the treatment of intracranial aneurysms. Once applied to whole blood, this treatment can be used to extend the effectiveness of endovascular coiling in an intracranial aneurysm. The next step in creating this treatment will be to repeat these experiments on whole blood and to move to *in vivo* studies in animals.

**Acknowledgements:** Special thanks to Maddie Cramer, Aimon Iftikhar, and Chase Webb.

## Sabrina Liu

Advisor: Adam Feinberg, Ph.D.  
Carnegie Heart

### Tracking cell-generated compaction strains in 3D tissue using fibronectin based nanomechanical biosensors

**Introduction:** Intra and intercellular forces play a major role in tissue growth, morphogenesis, and function. Initial geometric constraints and cytoskeletal interaction with the extracellular matrix influence changes in tissue morphology. To further investigate tissue development over time, we integrated a fluorescent fibronectin (FN) mesh with a 3D tissue construct that had an evolving morphology. Cell and gel constructs were cast in molds containing two upright posts that provided a stress field that promoted uniaxial alignment of tissue and formed a dogbone shape. Fluorescently labeled FN nanomechanical biosensors (NMBS) were fabricated to track tissue construct compaction over time, and a protocol was developed to transfer and track NMBS on the self-assembling tissue. A MATLAB code was created to analyze images of NMBS from confocal microscopy to determine segments of tension, compression, strain, and stress. Understanding the biomechanical forces that play a role in 3D tissue formation is a necessary step in improving strategies to engineer functional tissues for regenerative medicine applications.

**Materials and Methods:** Molds with the two-posts were designed using Solidworks and 3D printed with ABS. Polydimethylsiloxane (PDMS) was poured into the 3D-printed mold negatives, degassed, and allowed to cure. Before use, molds were sonicated in 50% ethanol, attached to 6-well plates using vacuum grease, incubated with 1% pluronics, and washed with 1x phosphate buffered saline. Collagen I (Col I) gels were cast at a final concentration of 4 mg/ml with 20% Matrigel™ and C2C12 myoblasts at a final seeding density of 15 million cells/mL. 50  $\mu$ L of gel solution was pipetted into each well of the PDMS mold and allowed to gel at 37° C. NMBS were fabricated using surface initiated assembly<sup>1</sup> using a 2:3 ratio of Alexa Fluor 546 labeled FN to unlabeled FN at 50  $\mu$ g/mL on PIPAAm. NMBS meshes have an initial pattern of 10  $\mu$ m line widths and 20x20  $\mu$ m spacing between. The coverslips patterned with NMBS were released onto gelatin via immersion in ddH<sub>2</sub>O and dissolution of PIPAAm. NMBS were transferred to the top of the PDMS molds and allowed to melt at 37° C to transfer NMBS to the Col I tissue construct. Phase contrast microscopy was used to track compaction of the 3D tissue, and confocal microscopy was used to track the fluorescent NMBS.

**Results and Discussion:** NMBS were found to remain intact for up to 7 days on a Col I gel control and 3 days on the 3D tissue, likely due to inadequate attachment of NMBS or matrix metalloproteinase (MMP) activity. Matrigel™ increased tissue compaction over 15% on Day 1 when compared to controls without Matrigel™. With NMBS attachment, Matrigel™ increased compaction on Day 1 by about 19%. The addition of Matrigel™ further stimulated compaction without interfering with the NMBS. Additionally, NMBS more effectively adhered to the Col I when gelatin and Col I were similar in temperature and elasticity during NMBS transfer.

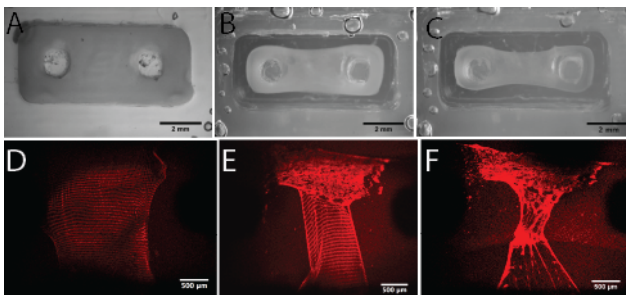


**Figure 1.** 3D tissue compaction progression at Day 0 (A), Day 2 (B), and Day 4 (C) imaged with phase contrast microscopy. Scale bar is 2 mm. NMBS (D-F) corresponds to each respective day and contracts with tissue. Scale bar is 500  $\mu$ m.

**Conclusions:** We have developed a method to transfer NMBS to an *in vitro* tissue construct that undergoes morphological changes, and we have been able to correlate changes in the NMBS to macroscopic changes in tissue compaction. Future studies include investigating methods to improve mesh integrity and inhibiting possible MMP activity responsible for mesh degradation, as well as improving imaging techniques. The development of NMBS placement technique can be applied to morphogenesis of other cell and gel tissue constructs, such as cardiomyocytes and human iPS, to gain greater understanding of the biomechanics of a tissue formation *in vitro*.

**Acknowledgements:** Special thanks to Alkiviadis Tsamis, Rebecca Duffy, and Thomas J Hinton.

**References:** [1] A.W. Feinberg, K.K. Parker. Surface-initiated assembly of protein nanofabrics. *Nano Lett.*, 10 (2010), pp. 2184–219.

**Rachel Freer,**

Advisor: Keith Cook, Ph.D.

Carnegie Heart

## Use of Factor XII Inhibitors to Reduce Coagulation on the Surface of Artificial Lung Devices

**Introduction:** Currently, artificial lungs only have the capability of lasting one or two weeks prior to failing due to clotting off. In order to extend the life capacity of these devices, preventing coagulation on the surface is imperative. As of now, the most common anti-coagulants stop coagulation at Factor X, which is the converging point of the coagulation cascade, which leaves the body unable to maintain physiological homeostasis conditions since it inhibits both the intrinsic and extrinsic pathways. In order to inhibit coagulation on artificial surfaces, only the intrinsic (contact) pathway needs to be inhibited, which is initiated by Factor XII (FXII). Thus, we will be looking into a new class of anti-coagulants that achieves this task. The aim of this research was two-fold. First, feasibility and cost of obtaining FXII inhibitors needed to be investigated. Because most of the Factor XII inhibitors are still in a state of research, they tend to be incredibly costly; thus, the second goal was to design a control circuit with minimal volume to minimize the amount of drug needed per circuit. Eventually, we hope to show that these Factor XII inhibitors extend the clotting time for artificial lung devices.

**Materials and Methods:** Companies that can produce custom proteins and aptamers were contacted to inquire about feasibility and cost of creating rHA-Infestin-4 and the FXII-specific aptamer respectively. The amounts of FXII inhibitor necessary were determined by analysis of APTT data in the current literature. Miniature lung devices were created by cutting 0.8” squares of 50% porosity fiber and melting them together into Chiclets comprised of five layers of fiber each. Eight Chiclets were placed into the housing and secured with end caps and silicone to complete each device. The devices were utilized in a minimal volume circuit comprised of Tygon tubing, which had inlet and outlet pressure readings. The flow rate was measured via weekly calibration of the pump. Sheep blood was used with a heparin dose of 2 units/mL of whole blood. The resistance was calculated utilizing the following equation:

$$R = \frac{\Delta P}{\text{flow rate}}$$

**Results and Discussion:** It was determined that both rHA-Infestin-4 and the FXII-specific aptamer will be able to be sourced from Genscript and TriLink BioTechnologies respectively. The amount of rHA-Infestin-4 necessary to run ten circuits is 46 mg, which was quoted to cost approximately \$30,000. The amount of aptamer necessary is 2 mg and we are currently awaiting the quote price. The aptamer likely requires less mass due to its highly specific nature. rHA-Infestin-4 has been shown to selectively bind to FXII, but also has the potential to bind to Factor Xa. The first circuit led to an adjustment of protocol. Based on a different circuit model, the circuit was primed with carbon dioxide, then saline, and finally blood. However, due to the small nature of the FXII inhibitor circuit, the saline diluted the blood, causing a hematocrit reading of only 14% red blood cells and a lack of resistance increase even after four hours. The second circuit clotted and failed after only 15 minutes. The hematocrit reading started at 26.5 and then dropped to 20 following mixing of saline with blood inside of the device. However, it is important to note that there was a delay in initiation of the pump due to a large amount of air bubbles within the circuit, so blood likely clotted in this time. The protocol was then solidified further with saline circuits to reduce air bubbles and the control blood circuits will resume in the near future.

**Conclusions:** For the future, we know how much of the Factor XII inhibitors are needed as well as their cost and a way to source them. A small circuit has been designed with a total volume of about 18 mL, which allows for minimization of the new class of anti-coagulant drugs. The protocol for the small circuit is still in the process of being perfected prior to testing the Factor XII inhibitors.

**Acknowledgements:** I would like to thank Dr. Cook for granting me the honor of working on this project, Kalli Bouloubassis for her immeasurable help and unwavering support, Caitlin Demarest for her guidance and patience throughout the process, as well as Chi Chi Do-Nguyen for being an incredible resource and helping along every step of the way.

## **Hsuan (Michelle) Ma**

Advisor: Dennis R Trumble, Ph.D.  
Carnegie Heart

### **Apical Torsion Device for Cardiac Support: Prototype Development**

#### **Introduction**

During contraction of a healthy heart, changes in muscle fiber orientation across the wall of the left ventricle cause the apex of the heart to turn 10–15 degrees in opposition to its base, creating a wringing motion. This cardiac motion, called LV torsion or ventricular twist, is believed to increase stroke volume, lower wall stress, and help the ventricles empty more completely. The lack of this ability in diseased hearts is associated with a variety of cardiac disease states. Therefore, it is reasonable to hypothesize that a torsion-based ventricular assist device (tVAD) could be used to restore this pumping action by “wringing” blood from both right and left ventricles concurrently. This could, in principle, be accomplished by attaching an actuator to the apex of the heart and powering the device electrically, pneumatically, or by low-volume hydraulics. The majority of commercial cardiac assist devices draw blood directly from the heart and pump it back to the circulatory system, which often leads to thromboembolic events, hemolysis, immune reactions, and infections due to intimate contact with the blood. The tVAD, in contrast, would minimize contact with the heart surface and avoid contact with the blood altogether.

#### **Materials and Methods**

The proposed tVAD prototype design consists of a device that captures and grips the apex of the heart. It is connected to a flexible drive shaft that traverses the chest wall and a rotary motor programmed to apply torsion during cardiac systole. A minimally invasive transcostal deployment system (no larger than a 5×5 cm square) should also be developed for device delivery and attachment. The prototype is currently modeled using 3D CAD software, i.e., Solidworks 2014. To achieve flexibility, the material chosen for the interface device is silicone rubber. To withstand mechanical torsion, the material chosen for the deployment system is 316L stainless steel.

#### **Results and Discussion**

The proposed interface device takes the form of a two-layer web, which is flexible and large enough to cover half of the ventricle surface from the apex. The inner surface of the web is attached to the epicardium with the aid of surgical glue as well as suction force for initial fixation. The outer layer of the web can be freely attached to and detached from the deployment system. The deployment system currently under development, about 3.5 cm in diameter, is introduced into the body through a small incision. It is composed of a shaft handle and a claw-shaped device that applies torsion to the apex. The claw-shaped device contains six fingers attached to the web, which expand and grip the apex, and features an actuator base connected to a driveshaft that contains a suction line for initial fixation. The fingers on the claw are sutured to and fixed between ridges on the web surface. The advantage of this design is that the fingers conform to the shape of the apex, allowing for a better grip. The ability to completely cover the apex of the ventricle also lowers shear stress and distributes pressure more evenly. In addition, the bilayer interface can be attached permanently to the apex using surgical glue, while the deployment system is made detachable so as to avoid damage to the epicardial tissue during device removal.

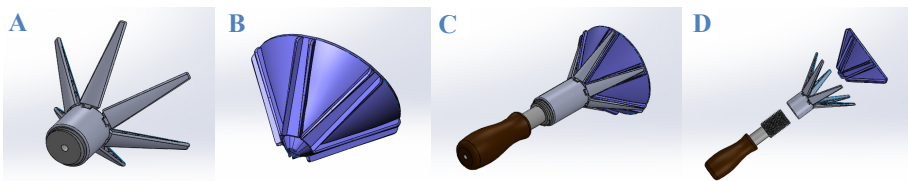


**Figure 1.** Solidworks Models of Prototype Design.

- (A) Claw-shaped device.
- (B) Interface device.
- (C) Assembly of (A), (B), and shaft handle.
- (D) Exploded view of (C).

#### **Conclusions**

The proposed interface and deployment design serves as an initial guide for tVAD prototype development. Research on adhesive and interface device material for this device is still needed, as are detailed design specifications describing the detachable deployment system. Further computational parametric studies and bench tests will be done to evaluate the most effective design parameters, including twisting angle, rotational speed, surface coverage, and myocardial stress distribution.

Acknowledgements: Special thanks to Elaine Sohoo for her support.

**Nicole Bustos**

Advisor: Cameron Riviere, Ph.D.

Carnegie Heart

**Considerations of a Spherical Surface Kinematics and Statics model for the Cerberus Epicardial Robot**

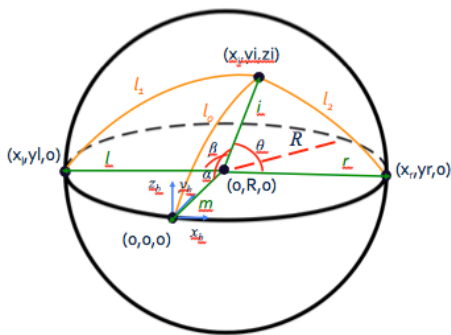
**Introduction:** Gene therapies are becoming prominent as a treatment for patients with congestive heart failure. The challenge facing heart failure gene therapy is not in finding an effective gene drug, rather the means of delivering it to the heart. The most efficient method of delivery is direct intramyocardial injections. However, the devices that deliver the injections can be inconsistent, and risky due to potential of perforation of the myocardial wall. Cerberus, a minimally invasive parallel wire robot for epicardial interventions, was developed for uniform delivery. Its flexible arms expand into a triangular shape and its three vertices suction onto the heart. Injections are possible from a frame of reference in which there is no myocardial motion. The injector head connected to wires from each base moves within the triangular shape formed by the bases by changing wire lengths.

The main concern for the device is to ensure stability for the patient as the therapies are delivered. To address this, previous work on Cerberus worked under simplified assumptions about the geometry of the robot and neglected the curvature of the heart, to derive inverse kinematics to yield wire lengths, and model the statics of the system. This paper presents work on enhancing the current kinematics and statics equations by modeling the device on a curved surface to reflect more realistic geometry.

**Materials and Methods:** Previous work included prototyping the device parts and a planar surface for testing the injector positioning and forces on the device. For the purposes of modeling the device to reflect more ideal conditions, a curved surface was constructed on SolidWorks from a pig heart model. The modeled device parts were also adjusted to fit to the new surface. An assembly of all the parts clearly reflects the change in geometry from the previous model.

To begin to form an algorithm for the curved surface, the surface is assumed as a sphere. Inverse kinematics can be found by treating the bases and injector as coordinate points and assuming that the middle main base is set as the origin using Cartesian coordinates. The shortest distance between two points, in this case the injector point and a base point, on the surface of a sphere is the “great-circle distance”. In non-Euclidean geometry, the geodesics on a sphere are the great circles whose centers correspond with the sphere center. Finding the angle between each base vector and the injector vector that all extend from the sphere center, the arc lengths of the wires can be found.

For the statics of the system, it is assumed that the mass of the injector is negligible. The system can be modeled such that the sum of the wire tensions will always be zero. The Cartesian coordinates are altered from the frame used in kinematics  $(x_b, y_b, z_b)$  with the middle base point as the origin to  $(x_i, y_i, z_i)$ , where the injector point serves as the origin so that the middle wire lines up with negative  $y_i$  and the normal force from the injector lines up with positive  $z_i$ .



**Results:** The following kinematics and statics equations were derived using the assumptions above, Fig 1, and Fig 2.

The lengths of the wires are given by:

$$\begin{bmatrix} l_0 \\ l_1 \\ l_2 \end{bmatrix} = \begin{bmatrix} R\alpha \\ R\beta \\ R\theta \end{bmatrix} = \begin{bmatrix} R\cos^{-1}\left(\frac{l \cdot i}{|l||i|}\right) \\ R\cos^{-1}\left(\frac{r \cdot i}{|r||i|}\right) \\ R\cos^{-1}\left(\frac{m \cdot i}{|m||i|}\right) \end{bmatrix}$$

Fig 1. Geometry and variables for IK

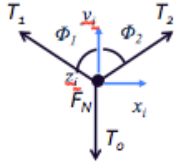


Fig 2. Free Body diagram of injector point

Resulting statics equations are given by:

$$\begin{aligned} \Sigma F_{x_i} &= T_1 \sin \phi_1 + T_r \sin \phi_r + T_m \sin \phi_m = 0 \\ \Sigma F_{y_i} &= T_1 \cos \phi_1 + T_r \cos \phi_r + T_m \cos \phi_m = 0 \\ \Sigma F_{z_i} &= F_N + T_i \sin \gamma_i + T_r \sin \gamma_r + T_m \sin \gamma_m = 0 \end{aligned}$$

**Conclusion:** The derived equations reflect more realistic device geometry, which can provide an algorithm for injector positioning on curved surface. Further work must consider diameter bases and injector size, as well as move onto an ellipsoid surface and then irregularly curved surfaces similar to the heart. Finally, movement of the heart should be considered so that the wires will adjust to with the motion while still maintaining correct tensions and stable injector.

**Acknowledgements:** I would like to thank Dr. Cameron N. Riviere, Nathan A. Wood, Adam D. Costanza, Dr. Michael J. Passineau, and Dr. Keith Cook.

**References:** Macauley S. Breault, Adam D. Costanza, Nathan A. Wood, Michael J. Passineau, and Cameron N. Riviere, "Toward Hybrid Force/Position Control for the Cerberus Epicardial Robot".

Macauley S. Breault, Adam D. Costanza, Nathan A. Wood, Michael J. Passineau, and Cameron N. Riviere, "Hybrid Control of an Epicardial Wire Robot".

## **Muyuan Li**

Advisors: Timothy Corcoran, Ph.D., Stephen Garoff, Ph.D., Todd Przybycien, Ph.D., and Robert Tilton, Ph.D.  
BME-SURP

### **Surfactant Driven Marangoni Flow on a Pre-deposited Lipid Monolayer**

#### **Introduction**

Marangoni flow is a spontaneous fluid flow when surface tension gradient exists on the fluid surface. Deposition of surfactant molecules to fluid surface causes a temporary uneven distribution of surfactant concentration, therefore leads to a surface tension gradient and consequently Marangoni flow on the surface. Surfactant induced Marangoni flow has been proposed to treat certain lung diseases. Regular aerosol drug delivery has a reduced efficiency on certain diseases that cause the blockage of lung by an abnormal excretion of mucus. With surfactant deposited together with the drug, drug particles are expected to penetrate the mucosal blockage and reach the targeted spot. However, the existence of a lipid layer in the lung might have unexpected effects on Marangoni spreading. Thus this study serves as a qualitative proof-of-concept for the proposed delivery mechanism.

#### **Material and Methods**

Surfactant driven spreading experiments on pre-deposited lipid monolayers are performed in this study. A lipid monolayer is deposited on a liquid sub-phase, then a constant sized drop of surfactant is deposited on the pre-deposited lipid layer. Spreading behavior of various lipid concentrations and surfactant types are recorded. Surface tension of the surface is recorded simultaneously with a Wilhelmy pin. Surfactants used are sodium dodecyl sulfate (SDS) and oleic acid. Experiments are performed in 14 cm Petri Dishes, with water as the sub-phase. Lipid used in the experiments is dipalmitoylphosphatidylcholine (DPPC), dissolved in chloroform. Fluid movement caused by the Marangoni flow is indicated by tracker particles. Polystyrene beads (~1 mm) and talc particles (< 10 μm) are the tracker particles used in the experiments. Movement of the tracker particles is video-recorded by a Nikon D3100 camera and analyzed with Nikon-NIS software.

#### **Results and Discussion**

Movement of polystyrene beads caused by surfactant driven Marangoni spreading is compared among different surface concentrations of DPPC. Both the time and amount of spreading change with lipids' surface concentration. Therefore spreading of the lipid-covered surface is determined by the surface tension gradient between the pre-deposited lipid layer and the secondary-deposited surfactant drop. Retraction of particles after maximum spreading is seen in spreading experiments with soluble surfactant but not with insoluble surfactants. Therefore the retraction is attributed to the dissolution of soluble surfactant into the sub-phase. Spreading caused by insoluble surfactant, with no retraction, is then hypothesized to have the form of piston movement, with the post-deposition surface having two distinct surfactant-only and lipid-only regions. Assuming the lipid is occupying the area covered by the talc and the clear area is covered by surfactant, a new lipid surface concentration can be calculated the corresponding surface tension of lipid monolayer can be found along the surface tension isotherm. Result shows that the calculated surface tension corresponds well with the measured surface tension by the Wilhelmy pin, and the surface tension of a surfactant monolayer (~40mN/m).

#### **Conclusion**

From the spreading experiments, it can be concluded that surfactant driven Marangoni flow on a pre-deposited lipid layer still is determined by the surface tension gradient. Marangoni flow induced by an insoluble surfactant acts as a piston of surfactant molecules pushing out the pre-deposited lipid molecules. Insoluble surfactants might be favored over soluble surfactants in application due to the absence of retraction.

## **Megan Pudlo**

Advisor: Keith Cook, Ph.D.

BME-SURP

### **Nitric Oxide Production from Silicone Fibers with Copper Catalyst**

Despite current methods for aided ventilation in diseased lungs such as extracorporeal membrane oxygenation (ECMO), practices like this are expensive and do not offer long term solutions for patients suffering from lung disease, an extremely relevant issue in today's society. In fact, Chronic Obstructive Pulmonary Disease (COPD) is the third leading cause of death in the United States and Cystic Fibrosis affects over thirty thousand Americans. The limited longevity of current solutions such as artificial oxygenators is often due to device failure from clotting. Clotting leads to a shortened period of viable use for the medical devices, ultimately reducing the effectiveness of them. In an attempt to combat the body's intrinsic pathway clotting response, this experiment utilizes silicone fibers coated in copper nanoparticles and supported by a polyvinyl alcohol (PVA) core. The copper serves as catalyst for the production of nitric oxide (NO) from donors in blood. Nitric oxide has localized antithrombotic effects since it diffuses into platelets and inhibits platelet activation and aggregation. Therefore, NO can reduce clotting responses. The production of nitric oxide was determined from fibers with 10% by weight of 50 nm copper particles. Fibers of known surface area had their PVA core dissolved and were attached to spinal needles using polydimethylsiloxane (PDMS). These fibers were then submerged in solution with glutathione (GSH), phosphate buffered solution, and a prepared NO donor, S-nitrosoglutathione (GSNO), to produce nitric oxide, which was swept from a reaction vessel into a Sievers Nitric Oxide Analyzer (NOA) by nitrogen gas and detected. By using the NOA to measure the nitrate concentrations of solutions with known concentrations, a calibration curve can be established. Utilizing the calibration curve, the nitric oxide flux produced from the fibers is determined. Proving that these fibers will produce a sufficient amount of nitric oxide to limit clotting would support the fiber's practicality in an artificial lung device. In conclusion, reducing platelet aggregation could increase the viability of artificial lung devices.